Published on 18 February 2015. Downloaded by Changchun Institute of Optics, Fine Mechanics and Physics, CAS on 29/05/2016 11:50:12.

Journal of Materials Chemistry A

PAPER

View Article Online
View Journal | View Issue

Cite this: J. Mater. Chem. A, 2015, 3, 6586

Electrospun Cr-doped $Bi_4Ti_3O_{12}/Bi_2Ti_2O_7$ heterostructure fibers with enhanced visible-light photocatalytic properties†

Hongfei Shi,[ab] Huaqiao Tan,*[ab] Wan-bin Zhu,[c] Zaicheng Sun,*[a] Yuejia Ma[a] and Enbo Wang*[b]

Received 8th December 2014
Accepted 16th February 2015

DOI: 10.1039/c4ta06736c

www.rsc.org/MaterialsA

A series of Cr-doped $Bi_4Ti_3O_{12}/Bi_2Ti_2O_7$ (BTO) heterostructure fibers have been synthesized *via* a one-step, facile and economical electrospinning/calcination process. SEM and TEM results reveal that the diameters of the as-prepared fibers are 100 ± 30 nm. The light adsorption of $Bi_4Ti_3O_{12}$ and $Bi_2Ti_2O_7$ in the fibers has been remarkably improved by Cr doping. With increased Cr doping, XRD and XPS show that the amount of $Bi_2Ti_2O_7$ increases in the fibers. As a result, the $Bi_4Ti_3O_{12}/Bi_2Ti_2O_7$ heterojunction structure is enhanced, which further promotes the charge separation of photogenerated charge carriers. Photocatalytic tests indicated that the as-prepared Cr-doped $Bi_4Ti_3O_{12}/Bi_2Ti_2O_7$ fibers exhibit good photocatalytic activity for photodegradation of methyl orange (MO) under visible-light irradiation.

Introduction

Recently, with increasing awareness of environmental deterioration and energy crisis, much effort has been directed to exploiting new semiconductor catalysts with high photocatalytic properties for environmental applications,[1–4] water splitting,[5,6] and CO_2 conversion.[7–10] Bi-based semiconductors such as BiOX (X = Cl, Br, I),[11] $BiVO_4$,[12] Bi_2WO_6,[13] Bi_2MoO_6,[14] Bi_2O_3,[15] Bi_2S_3 (ref. 16) and bismuth titanate,[17] as a new promising candidates for visible-light-driven catalysts are particularly interesting because of high photocatalytic performance.[18] Bismuth titanate is a large Bi–Ti–O family that includes several phases such as $Bi_{20}TiO_{32}$, $Bi_{12}TiO_{20}$, $Bi_2Ti_2O_7$, $Bi_4Ti_3O_{12}$ and $Bi_2Ti_4O_{11}$.[19] $Bi_{20}TiO_{32}$,[20] $Bi_{12}TiO_{20}$ (ref. 21) and $Bi_2Ti_2O_7$ (ref. 22) have been demonstrated as effective visible-light photocatalysts. $Bi_4Ti_3O_{12}$, a layered perovskite compound, is constructed by alternate stacking of $(Bi_2O_2)^{2+}$ layers and perovskite-like $(Bi_2Ti_3O_{10})^{2-}$ layers along the *c* axis.[23,24] Since Kudo and coworkers reported $Bi_4Ti_3O_{12}$ photocatalytic activity for water splitting,[25] $Bi_4Ti_3O_{12}$ has received much attention. This compound was usually synthesized by a solid-state reaction or a decomposition method. Both approaches have synthesis limitations due to nanostructural morphology with large surface areas and crystallinity. Therefore, a simpler and more rational method to obtain the nanostructured $Bi_4Ti_3O_{12}$ is in great demand.[26]

It is well known that electrospinning is one of the most convenient, universal and effective ways to prepare nanostructural compounds with diverse morphologies.[27,28] Very recently, Hu *et al.* demonstrated that electrospinning is a facile and effective method to synthesize 1D porous $Bi_4Ti_3O_{12}$ fibers.[29,30] But these synthesized $Bi_4Ti_3O_{12}$ fibers show relatively low visible-light photocatalytic activity because of their intrinsic properties such as wide band gap (3.0 eV) and low capability for separation of photogenerated charge carriers. To date, although many excellent works have been devoted to enhance the photocatalytic efficiency of $Bi_4Ti_3O_{12}$ under visible-light irradiation such as doping with metals[31–33] and combining with another narrow band gap semiconductor,[34–36] the development of high-efficiency visible-light-driven $Bi_4Ti_3O_{12}$ photocatalysts is still in great demand.

Herein, we describe fabricating a series of Cr-doped $Bi_4Ti_3O_{12}/Bi_2Ti_2O_7$ (BTO) heterostructure fibers *via* a one-step, facile and economical electrospinning/calcination route. The diameter of the nanofibers was 70–130 nm. The band gaps of $Bi_4Ti_3O_{12}$ and $Bi_2Ti_2O_7$ have been narrowed due to Cr doping, resulting in significant improvement of spectral absorption of fibers in visible light. In addition, with increased Cr doping, the amount of Bi_2TiO_7 increased in the electrospun fibers. As a result, the $Bi_4Ti_3O_{12}/Bi_2Ti_2O_7$ heterojunction structure was enhanced, which further promoted the charge separation of photogenerated charge carriers. Thus, the as-prepared photocatalysts exhibited remarkably enhanced visible-light photocatalytic activity for degradation of methyl orange (MO) compared to that of the initial $Bi_4Ti_3O_{12}/Bi_2Ti_2O_7$.

[a]State Key Laboratory of Luminescence and Applications, Changchun Institute of Optics, Fine Mechanics and Physics, Chinese Academy of Sciences, 3888 East Nanhu Road, Changchun 130033, People's Republic of China. E-mail: sunzc@ciomp.ac.cn

[b]Key Laboratory of Polyoxometalate Science of Ministry of Education, Department of Chemistry, Northeast Normal University, Ren Min Street No. 5268, Changchun, Jilin, 130024, People's Republic of China. E-mail: wangeb889@nenu.edu.cn

[c]State Key Laboratory of Applied Optics, Changchun Institute of Optics, Fine Mechanics and Physics, Chinese Academy of Sciences, Changchun 130033, China

† Electronic supplementary information (ESI) available: BET, XRD, UV-vis, XPS, transient photocurrent response, EIS. See DOI: 10.1039/c4ta06736c

This journal is © The Royal Society of Chemistry 2015

Published on 18 February 2015. Downloaded by Changchun Institute of Optics, Fine Mechanics and Physics, CAS on 29/05/2016 11:50:12.

Experimental

Chemicals and materials

$Bi(NO_3)_3 \cdot 5H_2O$, $Cr(NO_3)_3 \cdot 9H_2O$, tetrabutyl titanate (TBT), ethanol (CH_3CH_2OH), and *N*,*N*-dimethylformamide (DMF) were purchased from Aladdin Chemical Co., Ltd., China. Poly(vinylpyrrolidone) (PVP, MW ≈ 1 300 000) was obtained from Alfa Aesar. And all the chemicals were used without further purification.

Preparation of Cr-doped $Bi_4Ti_3O_{12}/Bi_2Ti_2O_7$ fibers

1.0 g of PVP was dissolved in 15 mL DMF/ethanol (volume ratio, 1 : 1) mixture solution. After stirring for 60 min, 2 mL glacial acetic acid, 0.97 g (2 mmol) of $Bi(NO_3)_3 \cdot 5H_2O$, 0.51 g (1.5 mmol) of TBT, $Cr(NO_3)_3 \cdot 9H_2O$ (0.01 g, 0.02 g, 0.04 g, 0.06 g and 0.08 g, respectively) were added to the solution. And then the mixture of PVP–$Bi(NO_3)_3 \cdot 5H_2O$–TBT–$Cr(NO_3)_3 \cdot 9H_2O$ was stirred until formation of clear solution. The solution was loaded into a 10 mL plastic syringe connected with a 22-gauge blunt needle. The solution feed rate was set at 0.5 mL h^{-1} controlled by a syringe pump. The metallic needle clamped with an electrode was connected to a variable high-voltage power supply, and an aluminium-foil collector was used as a grounded counter electrode 15 cm away from the needle tip. The PVP–$Bi(NO_3)_3 \cdot 5H_2O$–TBT–$Cr(NO_3)_3 \cdot 9H_2O$ composite fibers were formed at a high voltage of 15 kV. The electrospun precursor fibers were calcined at 600 °C with a heating rate of 2 °C min^{-1} in air for 1 h. By this method, the Cr-doped $Bi_4Ti_3O_{12}/Bi_2Ti_2O_7$ (BTO) nanofibers with different Cr contents (the amount of $Cr(NO_3)_3 \cdot 9H_2O$: 0.01 g, 0.02 g, 0.04 g, 0.06 g and 0.08 g, respectively) were fabricated and denoted as BTO-0.01, BTO-0.02, BTO-0.04, BTO-0.06 and BTO-0.08, respectively.

Characterization

The UV-vis absorption spectra were collected on a UV-2600 UV-vis spectrophotometer (Shimadzu), with an integrating sphere, and $BaSO_4$ was used as the reference. X-ray diffraction (XRD) analysis was recorded on a Bruker AXS D8 Focus using filtered Cu-Kα radiation (λ = 1.54056 Å). A JEOL JSM 4800F SEM coupled with an energy-dispersive X-ray (EDX) spectrometer was used to characterize sample morphology. High-resolution TEM (transmission electron microscopy) images were obtained *via* an FEI Tecnai G2 operated at 200 kV. XPS were carried out on an ESCALABMKII spectrometer with an Al-Kα (1486.6 eV) achromatic X-ray source. The PL spectra were recorded on a Hitachi F-7000 spectrophotometer. The excitation wavelength was 320 nm.

Photocatalytic degradation of methyl orange

The photocatalytic activities of the as-prepared samples were evaluated by degradation of methyl orange (MO) solution using a 300 W Xe lamp with a 420 nm cut-off filter as the light source and a self-made glass vessel with a water-cooling jacket as reactor. The irradiation distance between the lamp and the mixture solution was 15 cm. Forty milligrams of photocatalyst were dispersed in 40 mL 20 ppm of MO solution (pH = 1). Before irradiation, the solution was stirred in the dark for 60 min to ensure that the adsorption–desorption equilibrium between the organic molecules and the catalyst surface was reached. After irradiation for a designated time, 1.5 mL of the reaction solution was taken, centrifuged, and measured on a Shimadzu UV-vis spectrometer UV-2600 at a maximum absorption wavelength of 506 nm.

Photoelectrode preparation

According to the procedure in references,[37,38] electrophoretic deposition was used to place $Bi_4Ti_3O_{12}/Bi_2Ti_2O_7$ and BTO-0.08 on a FTO glass substrate, respectively. As shown in the following, 40 mg of as-prepared sample were dispersed in 50 mL of 0.2 mg mL^{-1} I_2/acetone solution under ultrasonic treatment. A two-electrode process was used to deposit the samples at 25 V for 15 min. Both electrodes were FTO glass substrates with the coated area about 1 × 4 cm^2. Then the deposited electrode was dried at 200 °C for 30 min to remove I_2 residue.

Photoelectrochemical measurements

The photoelectrochemical measurements of samples were investigated by a conventional three-electrode process in a quartz cell. A deposited BTO FTO photoanode, Pt foil and Hg/Hg_2Cl_2 electrode served as the working electrode, counter electrode and reference electrode, respectively. A 0.5 M Na_2SO_4 aqueous solution was used as the electrolyte. The photoanode was illuminated using a Beijing Trusttech Co., PLS-SXE-S500 300 W Xe lamp. The illuminated area was about 1 × 1 cm^2.

Results and discussion

Structural features and physical properties

The morphology and microstructure of the as-prepared $Bi_4Ti_3O_{12}/Bi_2Ti_2O_7$ and BTO-0.08 fibers are shown in Fig. 1. The SEM images display the fibers' relatively smooth and uniform surface before calcination. The average diameter of the fibers was about 150 ± 30 nm, and length as long as several millimeters. After annealing at 600 °C, the fibrous morphology of $Bi_4Ti_3O_{12}/Bi_2Ti_2O_7$ and BTO-0.08 fibers was well maintained. As shown in Fig. 1b and d, the diameters of the fibers were reduced to 100 ± 30 nm. And these fibers become coarse and porous. Transmission electron microscopy (TEM) images further provide the detailed microstructure of BTO-0.08. As shown in Fig. 1e, the BTO-0.08 fibers were composed of small nanoparticles about 30–60 nm in diameter. Owing to PVP decomposition during calcination, a porous structure was observed in the fibers. This porous structure is conducive to improvement of photocatalytic performance because it not only provides a large surface area for the catalysts but also offers many open channels that help reactants easily pass through it. The nitrogen adsorption–desorption isotherm curves of samples are shown in Fig. S1 and S2 in the ESI.† The BET surface areas of $Bi_4Ti_3O_{12}/Bi_2Ti_2O_7$, BTO-0.02, BTO-0.04 and BTO-0.08 were 6.681 $m^2 g^{-1}$, 15.102 $m^2 g^{-1}$, 16.263 $m^2 g^{-1}$ and 15.386 $m^2 g^{-1}$, respectively. Fig. 1f displays corresponding high-resolution

Published on 18 February 2015. Downloaded by Changchun Institute of Optics, Fine Mechanics and Physics, CAS on 29/05/2016 11:50:12.

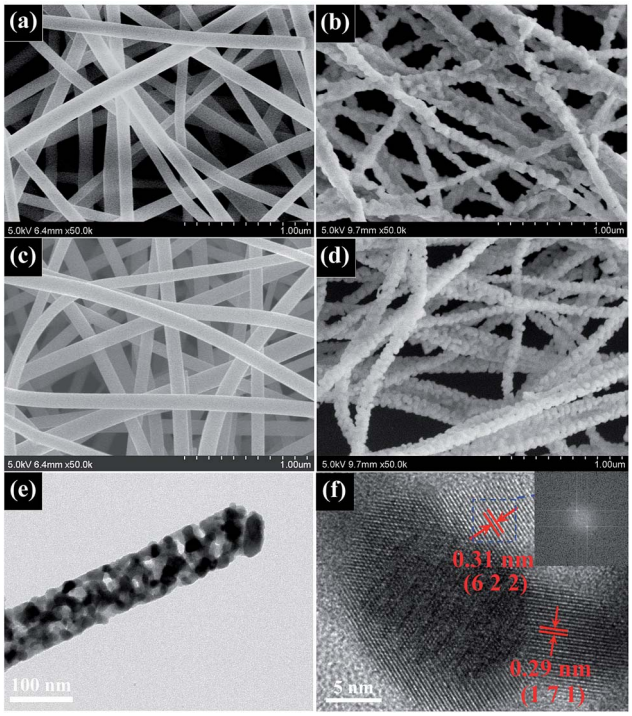

Fig. 1 SEM images of $Bi_4Ti_3O_{12}/Bi_2Ti_2O_7$ fibers (a) before calcination and (b) after calcination; (c) BTO-0.08 fibers before calcination and (d) after calcinations; TEM (e) and HRTEM (f) images for the BTO-0.08 sample. Inset in (f) is a corresponding FFT pattern.

TEM images and fast Fourier transform (FFT) images. The HRTEM images reveal that two independent crystal lattices, $Bi_4Ti_3O_{12}$ and $Bi_2Ti_2O_7$, were common. The lattice fringes observed corresponded to the interplanar distances of 0.29 nm and 0.31 nm, which could be assigned to the lattice spacing of $Bi_4Ti_3O_{12}$ (1 7 1) planes and $Bi_2Ti_2O_7$ (6 2 2) planes, respectively.

The optical properties of $Bi_4Ti_3O_{12}/Bi_2Ti_2O_7$ fibers and BTO fibers were measured by the UV-vis diffuse reflectance spectra in the range of 200–900 nm. As seen from the curves, the $Bi_4Ti_3O_{12}/Bi_2Ti_2O_7$ fibers exhibited an obvious spectra absorption onset at 400 nm, which was consistent with the band gap absorption edge of $Bi_4Ti_3O_{12}$. It showed little absorbance in the visible-light range. In contrast, the absorbance of the BTO fibers in visible light was improved. As seen in Fig. 2, additional absorption bands ranged from 400 nm to about 800 nm were observed. The absorbance intensity gradually increased with the increase in Cr dopant amount. The band gap of BTO samples was also narrowed from 3.1 eV to 2.4 eV gradually, as shown in Fig. S3.†

Fig. 3 shows the X-ray diffraction (XRD) pattern of the $Bi_4Ti_3O_{12}/Bi_2Ti_2O_7$ fibers and BTO fibers. The main diffraction peaks for the $Bi_4Ti_3O_{12}/Bi_2Ti_2O_7$ fibers can be assigned to orthorhombic $Bi_4Ti_3O_{12}$ (JCPDS 35-0795). Obviously, there are additional small diffraction peaks that can be attributed to cubic $Bi_2Ti_2O_7$ (JCPDS 32-0118). With increasing the amount of Cr doping, these small peaks gradually rose. In the crystal lattice of $Bi_4Ti_3O_{12}$ and $Bi_2Ti_2O_7$, Cr and Ti took the same position. The addition of Cr led to an increase in the Cr + Ti/Bi ratio.

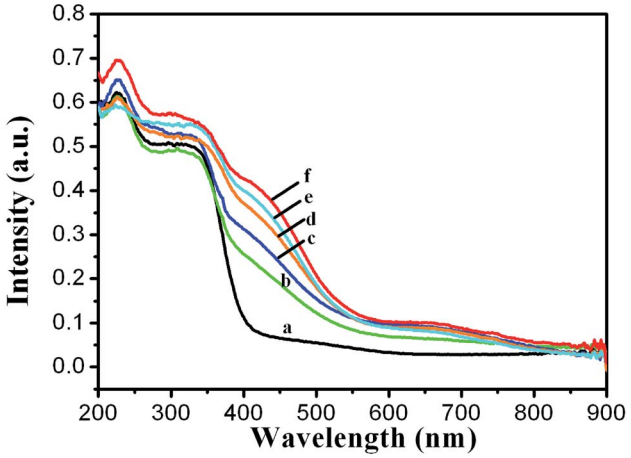

Fig. 2 UV-vis diffuse reflectance spectra of $Bi_4Ti_3O_{12}/Bi_2Ti_2O_7$ fibers and BTO fibers with different Cr contents. $Bi_4Ti_3O_{12}/Bi_2Ti_2O_7$ (a), BTO-0.01 (b), BTO-0.02 (c), BTO-0.04 (d), BTO-0.06 (e), and BTO-0.08 (f).

Therefore, the $Bi_2Ti_2O_7$ crystalline phase with higher Ti content could be further formed. As shown in BTO-0.08, the amount of $Bi_2Ti_2O_7$ in the electrospun fibers clearly increased. In summary, as Cr doping increased, the heterostructure of $Bi_4Ti_3O_{12}/Bi_2Ti_2O_7$ was enhanced. When more Cr(III) was added to the precursor, only Cr-doped $Bi_2Ti_2O_7$ was obtained after calcination (Fig. S4–S6†).

In order to investigate the composition and chemical state of the chromium-doped $Bi_4Ti_3O_{12}/Bi_2Ti_2O_7$, the energy-dispersive X-ray analysis (EDX) and X-ray photoelectron spectra (XPS) of $Bi_4Ti_3O_{12}/Bi_2Ti_2O_7$ fibers and BTO-0.08 were measured. Fig. 4a clearly exhibits the signals of Ti, Bi, O and Cr elements in the EDX pattern of BTO-0.08, indicating that Cr had doped into $Bi_4Ti_3O_{12}/Bi_2Ti_2O_7$ fibers successfully. This can be further confirmed by the XPS results. As shown in Fig. 4b, in BTO-0.08 the XPS signals originating from Cr 2p, O 1s, Ti 2p, C 1s and Bi 4f can be identified easily by the binding energies at 578 eV, 531

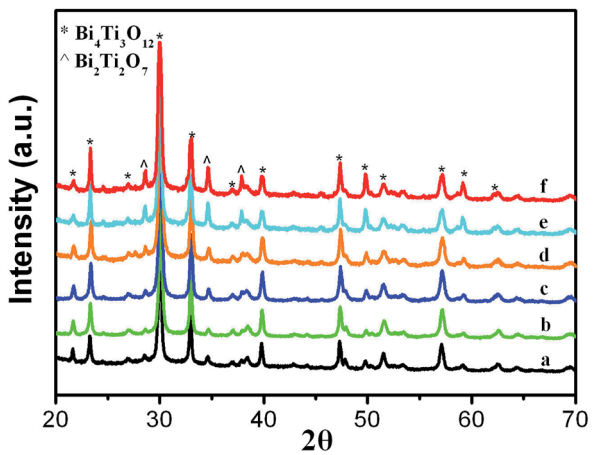

Fig. 3 XRD patterns of $Bi_4Ti_3O_{12}/Bi_2Ti_2O_7$ fibers and BTO fibers with different Cr contents. $Bi_4Ti_3O_{12}/Bi_2Ti_2O_7$ (a), BTO-0.01 (b), BTO-0.02 (c), BTO-0.04 (d), BTO-0.06 (e), and BTO-0.08 (f).

This journal is © The Royal Society of Chemistry 2015

Published on 18 February 2015. Downloaded by Changchun Institute of Optics, Fine Mechanics and Physics, CAS on 29/05/2016 11:50:12.

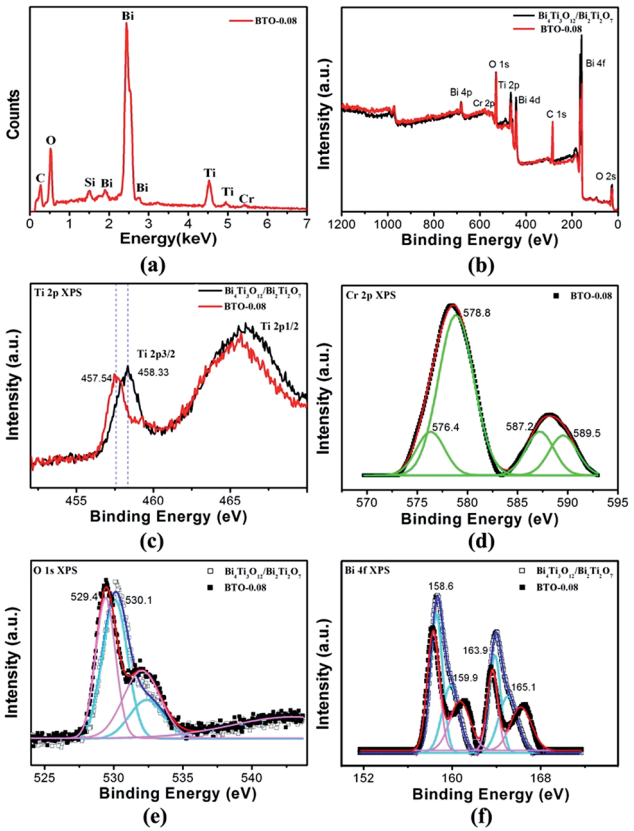

Fig. 4 (a) EDX spectra of BTO-0.08; (b) XPS spectra of $Bi_4Ti_3O_{12}/Bi_2Ti_2O_7$ and BTO-0.08; (c) Ti 2p XPS spectra of $Bi_4Ti_3O_{12}/Bi_2Ti_2O_7$ and BTO-0.08; (d) Cr 2p XPS spectra of BTO-0.08; (e) O 1s XPS spectra of $Bi_4Ti_3O_{12}/Bi_2Ti_2O_7$ and BTO-0.08; (f) Bi 4f XPS spectra of $Bi_4Ti_3O_{12}/Bi_2Ti_2O_7$ and BTO-0.08.

eV, 465 eV, 284 eV and 169 eV, respectively. Both EDX and XPS results confirm that chromium-doped bismuth titanate fibers formed through this simple electrospinning and sintering process. Fig. 4c shows the Ti 2p XPS of $Bi_4Ti_3O_{12}/Bi_2Ti_2O_7$ and BTO-0.08. Clearly, the high-resolution Ti 2p XPS spectra of BTO-0.08 shifted towards low binding energy compared to that of $Bi_4Ti_3O_{12}/Bi_2Ti_2O_7$. As seen from the O 1s and Bi 4f XPS spectra, some similar shifts were also observed that might have been caused by the presence of Cr doping. Fig. 4d and S7† show the Cr 2p XPS spectra of BTO-0.08. The two peaks of Cr $2p_{3/2}$ and Cr $2p_{1/2}$ can be split into Cr(III) and Cr(VI) at 576.4 eV, 587.2 eV (Cr(III)) and 578.8 eV, 589.5 eV (Cr(VI)), respectively.[39] The O 1s spectra of $Bi_4Ti_3O_{12}/Bi_2Ti_2O_7$ can be fitted into two Gaussian peaks at 530.1 eV and 532.4 eV, which can be assigned to Bi–O and Ti–O bonds, respectively.[30] And as shown in Fig. 4e, after Cr doping, the peak corresponding to Ti–O bonds showed an increase. This result was consistent with the XRD results. With the increase Cr contents, the $Bi_2Ti_2O_7$ phase that contained more Ti–O bonds increased gradually. The Bi 4f XPS spectra further confirmed the fact. As shown in Fig. 4f, two new shoulders at around 161.0 eV and 166.6 eV were observed in BTO-0.08, which can be attributed to the Cr-doped $Bi_2Ti_2O_7$. As Cr doping was added, the peaks of $Bi_2Ti_2O_7$ at 159.9 eV and 165.1 eV were shifted to 160.7 eV and 166.2 eV, respectively. Simultaneously, the ratio of peaks at high binding energy ($Bi_2Ti_2O_7$) and at low binding energy ($Bi_4Ti_3O_{12}$) increased, indicating that the amount of $Bi_2Ti_2O_7$ increased as the amount of Cr doping increased.

Photocatalytic activity, photocurrent response and photoluminescence spectra

The photocatalytic degradation of MO under visible-light irradiation ($\lambda > 420$ nm) had been chosen as a model reaction to evaluate the photocatalytic activities of $Bi_4Ti_3O_{12}/Bi_2Ti_2O_7$ and BTO fibers. Fig. 5a shows the time profiles of MO photocatalytic degradation over $Bi_4Ti_3O_{12}/Bi_2Ti_2O_7$ and BTO fibers under visible-light irradiation. Because these as-prepared samples were mesoporous materials, an obvious adsorption of MO on the fibers was observed in all cases before irradiation. And with the increased Cr content in fibers, adsorption was enhanced, which might be related to the larger surface area and surface charge changes of BTO. In the case of BTO-0.08, over 50% MO molecules were absorbed on the surface of BTO-0.08 fibers after stirring in the dark for 30 min. Under the visible-light irradiation, there was negligible self-photodegradation of MO. For $Bi_4Ti_3O_{12}/Bi_2Ti_2O_7$, only 4.8% of MO was degraded after irradiation under visible light for 5 h, because of its lower visible-light adsorption. The photocatalytic performances of BTO fibers were influenced by Cr doping content. With the increase amount of Cr, the photocatalytic activity of the BTO fibers was enhanced. As shown in Fig. 5a, the degradation efficiency of MO by BTO-0.01 (b), BTO-0.02 (c) and BTO-0.04 (d) was about 18.9%, 39.4% and 61.9% respectively irradiated under visible light for 5

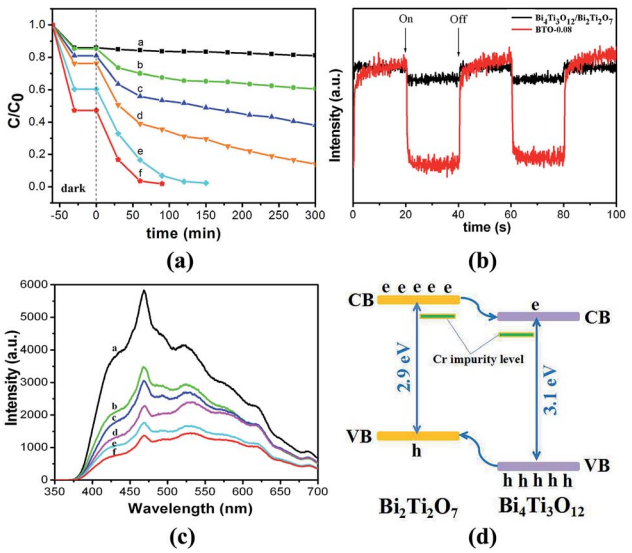

Fig. 5 (a) Degradation profiles of MO, using $Bi_4Ti_3O_{12}/Bi_2Ti_2O_7$ [a], BTO-0.01 [b], BTO-0.02 [c], BTO-0.04 [d], BTO-0.06 [e], and BTO-0.08 [f] as photocatalyst, where C is the concentration of MO and C_0 is the initial concentration of MO. (b) Transient photocurrent response of $Bi_4Ti_3O_{12}/Bi_2Ti_2O_7$ and BTO-0.08 in 0.5 M Na_2SO_4 aqueous solutions under visible-light irradiation at 0 V *vs.* Hg/Hg_2Cl_2. (c) PL spectra for $Bi_4Ti_3O_{12}/Bi_2Ti_2O_7$ [a], BTO-0.01 [b], BTO-0.02 [c], BTO-0.04 [d], BTO-0.06 [e], and BTO-0.08 [f]. (d) Schematic representation of band edges of Cr-doped $Bi_4Ti_3O_{12}/Bi_2Ti_2O_7$.

Published on 18 February 2015. Downloaded by Changchun Institute of Optics, Fine Mechanics and Physics, CAS on 29/05/2016 11:50:12.

h. For BTO-0.06 (e) and BTO-0.08 (f) (Fig. S8†), the MO molecules were almost degraded completely (the efficiency reach 98%) after visible-light irradiation for 150 min and 90 min respectively. Although degradation efficiency might be influenced by the initial adsorption, the kinetic linear simulation curves of MO photodegradation can directly reveal the photocatalytic activity of these BTO fibers. As shown in Fig. S9,† using the initial concentration of the MO after adsorption–desorption equilibrium as C_0, the calculated curves of k for degradation using $Bi_4Ti_3O_{12}/Bi_2Ti_2O_7$, BTO-0.01, BTO-0.02, BTO-0.04, BTO-0.06 and BTO-0.08 as the catalyst were 1.73634×10^{-4}, 8.8116×10^{-4}, 0.00206, 0.00494, 0.023 and 0.03745 min^{-1}, respectively. Clearly, BTO-0.08 possessed the highest photocatalytic activity under visible-light irradiation, owing to its enhanced visible-light response. Fig. S10† shows the cycling runs using BTO-0.08 as catalyst for photodegradation of MO under visible-light irradiation. With the process of recycle, the initial concentration of the MO after adsorption–desorption equilibrium was increased gradually, which might be influenced by the absorbed MO molecules on the BTO fibers. Recycled BTO fibers have lower absorbance capability than initial blank BTO fibers, because of the loss of sample recycling and the surface charge changes of BTO fibers. However, the photodegradation efficiency of three runs was all about 50% after visible-light irradiation for 90 min. That means BTO-0.08 had good stability.

In order to verify the enhanced visible-light photocatalytic activity and improved charge separation of BTO fibers, the transient photocurrent responses and the photoluminescence (PL) emission spectra of $Bi_4Ti_3O_{12}/Bi_2Ti_2O_7$ and BTO-0.08 were measured. As shown in Fig. 5b, both $Bi_4Ti_3O_{12}/Bi_2Ti_2O_7$ and BTO-0.08 fibers had an enhanced reproducible photocurrent response under visible-light irradiation when the light was switched on and off. The photocurrent density of BTO-0.08, 6.053×10^{-5} mA cm^{-2}, was 8 times higher than that of $Bi_4Ti_3O_{12}/Bi_2Ti_2O_7$ (7.47×10^{-6} mA cm^{-2}), implying that the visible-light photocatalytic activity and the charge separation of BTO-0.08 was significantly enhanced (Fig. S11 and S12†). This can be attributed to the improvement of visible-light adsorption and the enhanced heterojunction structures after Cr doping. Fig. 5c shows the PL spectra of $Bi_4Ti_3O_{12}/Bi_2Ti_2O_7$, BTO-0.02 and BTO-0.08 fibers. With an excitation wavelength at 320 nm, the emission intensity of BTO-0.02 and BTO-0.08 fibers was reduced, when compared with that of $Bi_4Ti_3O_{12}/Bi_2Ti_2O_7$. The BTO-0.08 had the largest decrease in PL peak density. These results revealed that the recombination of photogenerated charge carriers can be effectively inhibited when Cr doped. Fig. 5d shows the possible schematic representation of the band edges of Cr-doped $Bi_4Ti_3O_{12}/Bi_2Ti_2O_7$. As seen *via* XRD and XPS, when Cr was added, some of Ti centers could be substituted by Cr, which led to the increased amount of Ti/Bi, resulting in the further formation of $Bi_2Ti_2O_7$. With the increased contents of $Bi_2Ti_2O_7$, the type II heterojunction structure of $Bi_4Ti_3O_{12}/Bi_2Ti_2O_7$ was enhanced. The recombination of photogenerated charge carriers was effectively inhibited. Furthermore, $Bi_2Ti_2O_7$ possessed a band gap of 2.9 eV,[40] which can improve the light adsorption of $Bi_4Ti_3O_{12}$. On the other hand, when Cr doped, the spectra response of $Bi_4Ti_3O_{12}$ and $Bi_2Ti_2O_7$ could also be further extended. Therefore, the Cr-doped $Bi_4Ti_3O_{12}/Bi_2Ti_2O_7$ fibers showed good photocatalytic performance.

Conclusions

In summary, we fabricated a series of Cr-doped $Bi_4Ti_3O_{12}/Bi_2Ti_2O_7$ heterostructure fibers by a one-step, facile and economical electrospinning/calcination route. SEM and TEM revealed that the diameter of as-prepared fibers was about 100 ± 30 nm. With the increase in Cr content, the light adsorption of $Bi_4Ti_3O_{12}$ and $Bi_2Ti_2O_7$ was improved. The amount of $Bi_2Ti_2O_7$ in the fibers has been also raised, thus enhancing the type II heterojunction structure of $Bi_4Ti_3O_{12}/Bi_2Ti_2O_7$. The photogenerated charge separation of these Cr-doped BTO fibers was further enhanced. Therefore, photocatalytic tests displayed that the as-prepared Cr-doped $Bi_4Ti_3O_{12}/Bi_2Ti_2O_7$ fibers exhibited good photocatalytic activity for photodegradation of methyl orange (MO) under visible-light irradiation.

Acknowledgements

The authors thank the National Natural Science Foundation of China (21301166, 21201159, and 61176016), Science and Technology Department of Jilin Province (20130522127JH and 20121801). Z.S. is grateful for support by the CAS's "Hundred Talent Program." Supported by the open research fund program of the State Key Laboratory of Luminescence and Applications (Changchun Institute of Optics, Fine Mechanics and Physics, CAS) and Key Laboratory of Functional Inorganic Material Chemistry (Heilongjiang University), Ministry of Education, P. R. China.

Notes and references

1 M. R. Hoffmann, S. T. Martin, W. Choi and D. W. Bahnemann, *Chem. Rev.*, 1995, **95**, 69–96.
2 J. Lasek, Y. Yu and J. C. S. Wu, *J. Photochem. Photobiol., C*, 2013, **14**, 29–52.
3 C. Chen, W. Ma and J. Zhao, *Chem. Soc. Rev.*, 2010, **39**, 4206–4219.
4 H. Wang, L. Zhang, Z. Chen, J. Hu, S. Li, Z. Wang, J. Liu and X. Wang, *Chem. Soc. Rev.*, 2014, **43**, 5234–5244.
5 X. Chen, S. Shen, L. Guo and S. S. Mao, *Chem. Rev.*, 2010, **110**, 6503–6570.
6 Q. Li, B. Guo, J. Yu, J. Ran, B. Zhang, H. Yan and J. R. Gong, *J. Am. Chem. Soc.*, 2011, **133**, 10878–10884.
7 (*a*) Q. Xiang, J. Yu and M. Jaroniec, *J. Am. Chem. Soc.*, 2012, **134**, 6575–6578; (*b*) M. Marszewski, S. Cao, J. Yu and M. Jaroniec, *Mater. Horiz.*, 2015, DOI: 10.1039/c4mh00176a.
8 J. Yu, J. Low, W. Xiao, P. Zhou and M. Jaroniec, *J. Am. Chem. Soc.*, 2014, **136**, 8839–8842.
9 W. Ong, L. Tan, S. Chai and S. Yong, *Chem. Commun.*, 2015, **51**, 858–861.
10 X. Li, J. Yu, J. Low, Y. Fang, J. Xiao and X. Chen, *J. Mater. Chem. A.*, 2015, **3**, 2485–2534.
11 H. Cheng, B. Huang and Y. Dai, *Nanoscale*, 2014, **6**, 2009–2026.

 This journal is © The Royal Society of Chemistry 2015

Published on 18 February 2015. Downloaded by Changchun Institute of Optics, Fine Mechanics and Physics, CAS on 29/05/2016 11:50:12.

12 R. Li, H. Han, F. Zhang, D. Wang and C. Li, *Energy Environ. Sci.*, 2014, **7**, 1369–1376.
13 J. Tian, Y. Sang, G. Yu, H. Jiang, X. Mu and H. Liu, *Adv. Mater.*, 2013, **25**, 5075–5080.
14 H. Li, J. Liu, W. Hou, N. Du, R. Zhang and X. Tao, *Appl. Catal., B*, 2014, **160**, 89–97.
15 Z. Zhao, J. Tian, D. Wang, X. Kang, Y. Sang, H. Liu, J. Wang, S. Chen, R. I. Boughton and H. Jiang, *J. Mater. Chem.*, 2012, **22**, 23395–23403.
16 X. Gao, H. B. Wu, L. Zheng, Y. Zhong, Y. Hu and X. W. Lou, *Angew. Chem., Int. Ed.*, 2014, **53**, 5917–5921.
17 Y. Liu, M. Zhang, L. Li and X. Zhang, *Appl. Catal., B*, 2014, **160**, 757–766.
18 R. He, S. Cao, P. Zhou and J. Yu, *Chin. J. Catal.*, 2014, **35**, 989–1007.
19 Y. Li, L. Dang, L. Han, P. Li, J. Wang and Z. Li, *J. Mol. Catal. A: Chem.*, 2013, **379**, 146–151.
20 P. Hao, Z. Zhao, J. Tian, Y. Sang, G. Yu, H. Liu, S. Chen and W. Zhou, *Acta Mater.*, 2014, **62**, 258–266.
21 J. Hou, R. Cao, S. Jiao, H. Zhu and R. V. Kumar, *Appl. Catal., B*, 2011, **104**, 399–406.
22 J. Hou, S. Jiao, H. Zhu and R. V. Kumar, *J. Solid State Chem.*, 2011, **184**, 154–158.
23 W. Zhao, Z. Jia, E. Lei, L. Wang, Z. Li and Y. Dai, *J. Phys. Chem. Solids*, 2013, **74**, 1604–1607.
24 W. F. Yao, X. H. Xu, H. Wang, J. T. Zhou, X. N. Yang, Y. Zhang, S. X. Shang and B. B. Huang, *Appl. Catal., B*, 2004, **52**, 109–116.
25 A. Kudo and S. Hijii, *Chem. Lett.*, 1999, **28**, 1103–1104.
26 X. Lin, P. Lv, Q. Guan, H. Li, H. Zhai and C. Liu, *Appl. Surf. Sci.*, 2012, **258**, 7146–7153.
27 P. S. Kumar, J. Sundaramurthy, S. Sundarrajan, V. J. Babu, G. Singh, S. I. Allakhverdiev and S. Ramakrishna, *Energy Environ. Sci.*, 2014, **7**, 3192–3222.
28 C.-L. Zhang and S.-H. Yu, *Chem. Soc. Rev.*, 2014, **43**, 4423–4448.
29 D. Hou, W. Luo, Y. Huang, J. C. Yu and X. Hu, *Nanoscale*, 2013, **5**, 2028.
30 D. Hou, X. Hu, P. Hu, W. Zhang, M. Zhang and Y. Huang, *Nanoscale*, 2013, **5**, 9764–9772.
31 X. Lin, Q. Guan, Y. Zhang, T. Liu, C. Zou, C. Liu and H. Zhai, *J. Phys. Chem. Solids*, 2013, **74**, 1254–1262.
32 W. F. Yao, H. Wang, X. H. Xu, X. N. Yang, Y. Zhang, S. X. Shang and M. Zhang, *Appl. Catal., A*, 2003, **251**, 235–239.
33 J. Hou, R. Cao, Z. Wang, S. Jiao and H. Zhu, *J. Mater. Chem.*, 2011, **21**, 7296–7301.
34 W. Zhao, Y. Jin, C. H. Gao, W. Gu, Z. M. Jin, Y. L. Lei and L. S. Liao, *Mater. Chem. Phys.*, 2014, **143**, 952–962.
35 K. Chen, R. Hu, X. Feng, K. Xie, Y. Li and H. Gu, *Ceram. Int.*, 2013, **39**, 9109–9114.
36 X. B. Meng, J. Miao, Y. Zhao, S. Z. Wu, X. G. Xu, S. G. Wang and Y. Jiang, *J. Mater. Sci.: Mater. Electron.*, 2014, **25**, 1423–1428.
37 G. Liu, L.-C. Yin, J. Wang, P. Niu, C. Zhen, Y. Xie and H.-M. Cheng, *Energy Environ. Sci.*, 2012, **5**, 9603–9610.
38 H. Yu, Y. Zhao, C. Zhou, L. Shang, Y. Peng, Y. Cao, L.-Z. Wu, C.-H. Tung and T. Zhang, *J. Mater. Chem. A*, 2014, **2**, 3344–3351.
39 K. M. Parida, A. Nashim and S. K. Mahanta, *Dalton Trans.*, 2011, **40**, 12839–12845.
40 W. Wei, Y. Dai and B. Huang, *J. Phys. Chem. C*, 2009, **113**, 5658–5663.